Inorganic Chemistry
Article

Inorg. Chem. **2010**, *49*, 531–540 **531**
DOI: 10.1021/ic9015788

Excited-State Properties of Octahedral Hexarhenium(III) Complexes with Redox-active N-heteroaromatic Ligands

Takashi Yoshimura,*,† Chiaki Suo,† Kiyoshi Tsuge,† Shoji Ishizaka,‡ Koichi Nozaki,§ Yoichi Sasaki,‡,∥ Noboru Kitamura,‡ and Atsushi Shinohara†

†*Department of Chemistry, Graduate School of Science, Osaka University, Toyonaka, Osaka 560-0043, Japan,* ‡*Department of Chemistry, Graduate School of Science, Hokkaido University, Sapporo 060-0810, Japan,* §*Department of Chemistry, Graduate School of Science and Engineering, Toyama University, Toyama 930-8555, Japan, and* ∥*Catalysis Research Center, Hokkaido University, Sapporo 001-0021, Japan*

Received August 7, 2009

New sulfide-capped octahedral hexarhenium(III) complexes containing 4-phenylpyridine (ppy) or 1,2-bis(4-pyridyl)ethane (bpe) $((n\text{-}C_4H_9)_4N)[mer\text{-}\{Re_6S_8Cl_3(ppy)_3\}]$ ((Bu_4N)[**1**]), $((n\text{-}C_4H_9)_4N)_2[trans\text{-}\{Re_6S_8Cl_4(ppy)_2\}]$ ($(Bu_4N)_2$[**2a**]), $((n\text{-}C_4H_9)_4N)_2[cis\text{-}\{Re_6S_8Cl_4(ppy)_2\}]$ ($(Bu_4N)_2$[**2b**]), $((n\text{-}C_4H_9)_4N)_2[trans\text{-}\{Re_6S_8Cl_4(bpe)_2\}]$ ($(Bu_4N)_2$[**3a**]), and $((n\text{-}C_4H_9)_4N)_2[cis\text{-}\{Re_6S_8Cl_4(bpe)_2\}]$ ($(Bu_4N)_2$[**3b**]) were prepared, and X-ray single-crystal structure determination was carried out for $(Bu_4N)_2$[**2a**] and $(Bu_4N)_2$[**3a**]. The photophysical properties of these complexes were studied both in acetonitrile at 298 K and in the solid state at 298 and 80 K, along with those of the known 4,4′-bipyridine (bpy) analogues $((n\text{-}C_4H_9)_4N)[mer\text{-}\{Re_6S_8Cl_3(bpy)_3\}]$ ((Bu_4N)[**4**]), $((n\text{-}C_4H_9)_4N)_2[trans\text{-}\{Re_6S_8Cl_4(bpy)_2\}]$ ($(Bu_4N)_2$[**5a**]), and $((n\text{-}C_4H_9)_4N)_2[cis\text{-}\{Re_6S_8Cl_4(bpy)_2\}]$ ($(Bu_4N)_2$[**5b**]). The photophysical data of $[\mathbf{5a}]^{2-}$ and $[\mathbf{5b}]^{2-}$ in solution and in the solid state were significantly different from those of other complexes. On the basis of experimental observations of $[\mathbf{2a}]^{2-}$ and $[\mathbf{5a}]^{2-}$ and density-functional theory (DFT) calculations, it was concluded that $[\mathbf{5a}]^{2-}$ and $[\mathbf{5b}]^{2-}$ exhibited metal (Re_6S_8 core)-to-ligand (bpy) charge transfer (MLCT) type emission. This is the first unambiguous demonstration of MLCT type emissions for the hexarhenium complexes. The MLCT components, where present, are only minor in the case of the emissions of $[\mathbf{1}]^-$, $[\mathbf{2a}]^{2-}$, $[\mathbf{2b}]^{2-}$, and $[\mathbf{4}]^-$; these can be explained primarily as the contributions of the intracore electronic transitions. The emissions of $[\mathbf{3a}]^{2-}$ and $[\mathbf{3b}]^{2-}$ can be assigned almost completely to the electronic transitions within the Re_6S_8 core. The different emission characteristics of the bis(bpy) complexes ($[\mathbf{5a}]^{2-}$ and $[\mathbf{5b}]^{2-}$) from the tris(bpy) complex ($[\mathbf{4}]^-$) are a result of the increase in the number of nitrogen donors on the Re_6S_8 core, which stabilizes the Re_6S_8 core energy to a lower level than the energy of the bpy ligand π^* orbital. On the other hand, it has been shown that the emissions of the bis(ppy) ($[\mathbf{2a}]^{2-}$ and $[\mathbf{2b}]^{2-}$) and bis(bpe) complexes ($[\mathbf{3a}]^{2-}$ and $[\mathbf{3b}]^{2-}$) are best characterized by the higher π^* energy level of each N-heteroaromatic ligand, which lead to a stronger metal character in the emissive excited state of the complex.

Introduction

Octahedral hexarhenium complexes with an Re_6Q_8 (Q = S, Se) core have attracted interest recently since they exhibit intriguing electrochemical, spectroscopic, and excited-state properties.[1−9] A number of neutral or anionic ligands such as phosphine,[10−24] N-heteroaromatic ligands,[18−33] carbonyl,[34,35] solvent molecules (CH_3CN, *N,N*-dimethylformamide (DMF), dimethylsulfoxide (DMSO), H_2O),[16−18,36−40] cyanide,[11,41−45] hydroxide,[25,37,39,46] isothiocyanide,[47] and carboxylate[48] have been introduced to the terminal positions of the Re_6Q_8 core. Further, hexarhenium(III) complexes with mixed terminal ligands are well-known. Most hexarhenium(III) complexes

*To whom correspondence should be addressed. E-mail: tyoshi@chem.sci.osaka-u.ac.jp. Phone: 81-6-6850-5416. Fax: 81-6-6850-5418.

(1) Fedorov, V. E.; Mironov, Y. V.; Naumov, N. G.; Sokolov, M. N.; Fedin, V. P. *Russ. Chem. Rev*. **2007**, *76*, 529–552.
(2) Gabriel, J.-C. P.; Boubekeur, K.; Uriel, S.; Batail, P. *Chem. Rev*. **2001**, *101*, 2037–2066.
(3) Gray, T. G. *Coord. Chem. Rev*. **2003**, *243*, 213–235.
(4) Saito, T. *J. Chem. Soc., Dalton Trans*. **1999**, 97–106.
(5) Sasaki, Y. *J. Nucl. Radiochem. Sci*. **2005**, *6*, 145–148.
(6) Sasaki, Y. *Bull. Jpn. Soc. Coord. Chem*. **2006**, *48*, 50.
(7) Selby, H. D.; Roland, B. K.; Zheng, Z. *Acc. Chem. Res*. **2003**, *36*, 933–944.
(8) Selby, H. D.; Zheng, Z. *Comments Inorg. Chem*. **2005**, *26*, 75–102.
(9) Welch, E. J.; Long, J. R. In *Progress in Inorganic Chemistry*.; John Wiley & Sons, Inc: New York, 2005; Vol. *54*, pp 1−45.
(10) Willer, M. W.; Long, J. R.; McLauchlan, C. C.; Holm, R. H. *Inorg. Chem*. **1998**, *37*, 328–333.
(11) Gray, T. G.; Holm, R. H. *Inorg. Chem*. **2002**, *41*, 4211–4216.
(12) Chen, Z.-N.; Yoshimura, T.; Abe, M.; Tsuge, K.; Sasaki, Y.; Ishizaka, S.; Kim, H.-B.; Kitamura, N. *Chem.—Eur. J*. **2001**, *7*, 4447–4455.
(13) Shestopalov, M. A.; Mironov, Y. V.; Brylev, K. A.; Kozlova, S. G.; Fedorov, V. E.; Spies, H.; Pietzsch, H.-J.; Stephan, H.; Geipel, G.; Bernhard, G. *J. Am. Chem. Soc*. **2007**, *129*, 3714–3721.
(14) Zheng, Z.; Tu, X. *CrystEngComm* **2009**, *11*, 707–719.
(15) Tu, X.; Nichol, G. S.; Zheng, Z. *J. Cluster Sci*. **2009**, *20*, 93–103.

Published on Web 12/15/2009

exhibit intense red emissions at room temperature in both solid and solution phases.[12,13,25−27,39,47−58] Typically, the maximum wavelength (λ_{em}) of the emission from a hexarhenium(III) complex in solution ranges from 650 to 800 nm with a lifetime (τ_{em}) of several microseconds at room temperature.[12,13,27,39,47−58] On the basis of the fairly long emission lifetimes and the insensitive nature of the emission spectrum to the type of solvents employed, it has been proposed that the emitting excited state of the hexarhenium(III) complex is a spin-triplet type and involves orbitals that are primarily localized on the Re_6Q_8 core.[47,50−55] In addition to these experimental observations, theoretical studies of the excited state of $[Re_6S_8X_6]^{4-}$ (X = Cl, Br, I, CN) have demonstrated that the lowest-energy unoccupied molecular orbitals (LUMOs) are primarily localized on the Re_6Q_8 core.[53,54,59−62]

In a previous study, we reported the emission properties of a series of μ_3-S capped hexarhenium(III) complexes with mixed terminal ligands, $[Re_6S_8Cl_4L_2]^{2-}$, where L was pyridine (py) or its derivatives.[27] It is worth emphasizing that the emission properties of these complexes are largely dependent on the nature of L. While $[Re_6S_8Cl_4L_2]^{2-}$ with py or 4-methylpyridine (mpy) as L is highly luminescent in acetonitrile at room temperature (the emission quantum yield (Φ_{em}) = 0.033−0.042 for the py complex and 0.031−0.057 for the mpy analogue), the complex with unidentate 4,4′-bipyridine (bpy) or pyrazine (pz) as L is only weakly luminescent (Φ_{em} = 0.0011−0.0013 for $[Re_6S_8Cl_4(bpy)_2]^{2-}$ or 0.0010−0.0017 for $[Re_6S_8Cl_4(pz)_2]^{2-}$).[27] Hence, it is concluded that the emissive excited triplet states of the complexes in the former group are primarily localized on the Re_6S_8 core since their λ_{em}, Φ_{em}, and τ_{em} values are similar to those of $[Re_6S_8X_6]^{4-}$ (X = Cl, Br, I, CN, or NCS).[47] To consider the origin of the weak emission properties of $[Re_6S_8Cl_4(bpy)_2]^{2-}$ and $[Re_6S_8Cl_4(pz)_2]^{2-}$, two points must be noted. One is the redox-active nature of bpy and pz ligands. In fact, N-heteroaromatic ligand-centered reduction waves are observed at around −1.45 and −1.34 V (vs Ag/AgCl) for $[Re_6S_8Cl_4(bpy)_2]^{2-}$ and $[Re_6S_8Cl_4(pz)_2]^{2-}$, respectively.[27] Second, bpy and pz ligands in the relevant Re_6S_8 complex bear free coordination sites. On the basis of these viewpoints, we have suggested that the lowest-energy excited state that is responsible for the emission involves the N-heteroaromatic ligand-centered π^* orbital, and moreover, the interaction of the ligand with solvent molecules results in a quenching pathway for the emission.[27] Although the observation of the ligand reduction wave indicates that the LUMO of the complex is characterized by the ligand π^* orbital, this does

(16) Zheng, Z.; Long, J. R.; Holm, R. H. *J. Am. Chem. Soc.* **1997**, *119*, 2163–2171.
(17) Zheng, Z.; Holm, R. H. *Inorg. Chem.* **1997**, *36*, 5173–5178.
(18) Zheng, Z.; Gray, T. G.; Holm, R. H. *Inorg. Chem.* **1999**, *38*, 4888–4895.
(19) Roland, B. K.; Selby, H. D.; Cole, J. R.; Zheng, Z. *Dalton Trans.* **2003**, 4307–4312.
(20) Roland, B. K.; Carter, C.; Zheng, Z. *J. Am. Chem. Soc.* **2002**, *124*, 6234–6235.
(21) Roland, B. K.; Selby, H. D.; Carducci, M. D.; Zheng, Z. *J. Am. Chem. Soc.* **2002**, *124*, 3222–3223.
(22) Roland, B. K.; Flora, W. H.; Carducci, M. D.; Armstrong, N. R.; Zheng, Z. *J. Cluster Sci.* **2004**, *14*, 449–458.
(23) Roland, B. K.; Flora, W. H.; Armstrong, N. R.; Zheng, Z. *C. R. Chim.* **2005**, *8*, 1798–1807.
(24) Roland, B. K.; Flora, W. H.; Selby, H. D.; Armstrong, N. R.; Zheng, Z. *J. Am. Chem. Soc.* **2006**, *128*, 6620–6625.
(25) Dorson, F.; Molard, Y.; Cordier, S.; Fabre, B.; Efremova, O.; Rondeau, D.; Mironov, Y.; Circu, V.; Naumov, N.; Perrin, C. *Dalton Trans.* **2009**, 1297–1299.
(26) Shestopalov, M. A.; Cordier, S.; Hernandez, O.; Molard, Y.; Perrin, C.; Perrin, A.; Fedorov, V. E.; Mironov, Y. V. *Inorg. Chem.* **2009**, *48*, 1482–1489.
(27) Yoshimura, T.; Umakoshi, K.; Sasaki, Y.; Ishizaka, S.; Kim, H.-B.; Kitamura, N. *Inorg. Chem.* **2000**, *39*, 1765–1772.
(28) Yoshimura, T.; Umakoshi, K.; Sasaki, Y.; Sykes, A. G. *Inorg. Chem.* **1999**, *38*, 5557–5564.
(29) Selby, H. D.; Roland, B. K.; Carducci, M. D.; Zheng, Z. *Inorg. Chem.* **2003**, *42*, 1656–1662.
(30) Selby, H. D.; Orto, P.; Carducci, M. D.; Zheng, Z. *Inorg. Chem.* **2002**, *41*, 6175–6177.
(31) Selby, H. D.; Orto, P.; Zheng, Z. *Polyhedron* **2003**, *22*, 2999–3008.
(32) Itasaka, A.; Abe, M.; Yoshimura, T.; Tsuge, K.; Suzuki, M.; Imamura, T.; Sasaki, Y. *Angew. Chem., Int. Ed.* **2002**, *41*, 463–466.
(33) Selby, H. D.; Zheng, Z.; Gray, T. G.; Holm, R. H. *Inorg. Chim. Acta* **2001**, *312*, 205–209.
(34) Orto, P. J.; Nichol, G. S.; Wang, R.; Zheng, Z. *Inorg. Chem.* **2007**, *46*, 8436–8438.
(35) Orto, P. J.; Nichol, G. S.; Okumura, N.; Evans, D. H.; Arratia-Perez, R.; Ramirez-Tagle, R.; Wang, R.; Zheng, Z. *Dalton Trans.* **2008**, 4247–4253.
(36) Fedin, V. P.; Virovets, A. A.; Sykes, A. G. *Inorg. Chim. Acta* **1998**, *271*, 228–230.
(37) Zheng, Z.; Selby, H. D.; Roland, B. K. *Acta Crystallogr., Sect. E* **2001**, *E57*, i77–i79.
(38) Mironov, Y. V.; Yarovoi, S. S.; Naumov, D. Y.; Simon, A.; Fedorov, V. E. *Inorg. Chim. Acta* **2007**, *360*, 2953–2957.
(39) Brylev, K. A.; Mironov, Y. V.; Yarovoi, S. S.; Naumov, N. G.; Fedorov, V. E.; Kim, S.-J.; Kitamura, N.; Kuwahara, Y.; Yamada, K.; Ishizaka, S.; Sasaki, Y. *Inorg. Chem.* **2007**, *46*, 7414–7422.
(40) Orto, P.; Selby, H. D.; Ferris, D.; Maeyer, J. R.; Zheng, Z. *Inorg. Chem.* **2007**, *46*, 4377–4379.
(41) Mironov, Y. V.; Cody, J. A.; Albrecht-Schmitt, T. E.; Ibers, J. A. *J. Am. Chem. Soc.* **1997**, *119*, 493–498.
(42) Beauvais, L. G.; Shores, M. P.; Long, J. R. *Chem. Mater.* **1998**, *10*, 3783–3786.
(43) Naumov, N. G.; Ostanina, E. V.; Virovets, A. V.; Schmidtman, M.; Mueller, A.; Fedorov, V. E. *Russ. Chem. Bull.* **2002**, *51*, 866–871.
(44) Artemkina, S. B.; Naumov, N. G.; Virovets, A. V.; Fedorov, V. E. *J. Struct. Chem.* **2002**, *43*, 689–693.
(45) Naumov, N. G.; Ledneva, A. Y.; Kim, S.-J.; Fedorov, V. E. *J. Cluster Sci.* **2009**, *20*, 225–239.
(46) Yarovoi, S. S.; Mironov, Y. V.; Naumov, D. Y.; Gatilov, Y. V.; Kozlova, S. G.; Kim, S.-J.; Fedorov, V. E. *Eur. J. Inorg. Chem.* **2005**, 3945–3949.
(47) Yoshimura, T.; Chen, Z.-N.; Itasaka, A.; Abe, M.; Sasaki, Y.; Ishizaka, S.; Kitamura, N.; Yarovoi, S. S.; Solodovnikov, S. F.; Fedorov, V. E. *Inorg. Chem.* **2003**, *42*, 4857–4863.
(48) Brylev, K. A.; Mironov, Y. V.; Kozlova, S. G.; Fedorov, V. E.; Kim, S.-J.; Pietzsch, H.-J.; Stephan, H.; Ito, A.; Ishizaka, S.; Kitamura, N. *Inorg. Chem.* **2009**, *48*, 2309–2315.
(49) Guilbaud, C.; Deluzet, A.; Domercq, B.; Molinie, P.; Boubekeur, K.; Batail, P.; Coulon, C. *Chem. Commun.* **1999**, 1867–1868.
(50) Gray, T. G.; Rudzinski, C. M.; Nocera, D. G.; Holm, R. H. *Inorg. Chem.* **1999**, *38*, 5932–5933.
(51) Yoshimura, T.; Ishizaka, S.; Umakoshi, K.; Sasaki, Y.; Kim, H.-B.; Kitamura, N. *Chem. Lett.* **1999**, 697–698.
(52) Yoshimura, T.; Ishizaka, S.; Sasaki, Y.; Kim, H.-B.; Kitamura, N.; Naumov, N. G.; Sokolov, M. N.; Fedorov, V. E. *Chem. Lett.* **1999**, 1121–1122.
(53) Gray, T. G.; Rudzinski, C. M.; Meyer, E. E.; Holm, R. H.; Nocera, D. G. *J. Am. Chem. Soc.* **2003**, *125*, 4755–4770.
(54) Gray, T. G.; Rudzinski, C. M.; Meyer, E. E.; Nocera, D. G. *J. Phys. Chem. A* **2004**, *108*, 3238–3243.
(55) Kitamura, N.; Ueda, Y.; Ishizaka, S.; Yamada, K.; Aniya, M.; Sasaki, Y. *Inorg. Chem.* **2005**, *44*, 6308–6313.
(56) Kobayashi, N.; Ishizaka, S.; Yoshimura, T.; Kim, H.-B.; Sasaki, Y.; Kitamura, N. *Chem. Lett.* **2000**, 234–235.
(57) Chen, Z.-N.; Yoshimura, T.; Abe, M.; Sasaki, Y.; Ishizaka, S.; Kim, H.-B.; Kitamura, N. *Angew. Chem., Int. Ed.* **2001**, *40*, 239–242.
(58) Mironov, Y. V.; Shestopalov, M. A.; Brylev, K. A.; Yarovoi, S. S.; Romanenko, G. V.; Fedorov, V. E.; Spies, H.; Pietzsch, H.-J.; Stephan, H.; Geipel, G.; Bernhard, G.; Kraus, W. *Eur. J. Inorg. Chem.* **2005**, 657–661.
(59) Gray, T. G. *Chem.—Eur. J.* **2009**, *15*, 2581–2593.
(60) Roy, L. E.; Hughbanks, T. *Inorg. Chem.* **2006**, *45*, 8273–8282.
(61) Honda, H.; Noro, T.; Tanaka, K.; Miyoshi, E. *J. Chem. Phys.* **2001**, *114*, 10791–10797.
(62) Arratia-Perez, R.; Hernandez-Acevedo, L. *J. Chem. Phys.* **1999**, *110*, 2529–2532.

not necessarily guarantee that the emissive excited state is also ligand-centered. Therefore, it has been also suggested that the Re_6S_8 core-centered excited state responsible for the intense emission would be deactivated by electronic interactions of the Re_6S_8 core-centered excited state with the ligand π^* state.[27] Clearly, the role of the low-energy lying π^* orbital of an N-heteroaromatic ligand in the nature of the emissive excited state of a hexarhenium(III) complex must be elucidated.

The purpose of our study is to examine the roles of the Re_6S_8 core-to-N-heteroaromatic ligand charge-transfer (MLCT) interaction type and thereby the low-energy lying ligand-centered π^* orbital, as well as the role of the uncoordinated nitrogen site of the ligand in the spectroscopic and excited-state properties of $[Re_6S_8Cl_4L_2]^{2-}$ (L = bpy, pz). To achieve this, we studied detailed emission properties of *mer*-$[Re_6S_8Cl_3(bpy)_3]^-$, *trans*-/*cis*-$[Re_6S_8Cl_4(bpy)_2]^{2-}$, and new complexes of $[Re_6S_8Cl_{6-n}L_n]^{n-4}$, where L is 4-phenylpyridine (ppy) or 1,2-bis(4-pyridyl)ethane (bpe). 4-Phenylpyridine is redox-active and its redox potential of the compound is about +0.3 V, which is more negative than that of bpy or pz. A bpe ligand is potentially bidentate and redox inactive, and leaves a free nitrogen site when it coordinates to a Re_6S_8 core. On the basis of photophysical, spectroscopic, and electrochemical studies, together with molecular orbital (MO) calculations of the lowest-energy absorption band of *trans*-$[Re_6S_8Cl_4L_2]^{2-}$ (L = ppy or bpy), we demonstrate that the spectroscopic and photophysical properties of $[Re_6S_8Cl_4L_2]^{2-}$ (L = bpy or pz) are significantly affected by the availability of the charge transfer transition from the Re_6S_8 core to the π^* orbital of the N-heteroaromatic ligand.

Experimental Section

Materials. Hexarhenium(III) complexes, $(Bu_4N)_3[Re_6S_8Cl_6]$, (Bu_4N)[*mer*-$\{Re_6S_8Cl_3(bpy)_3\}$] ((Bu_4N)[**4**]), $(Bu_4N)_2$[*trans*-$\{Re_6S_8Cl_4(bpy)_2\}$] ($(Bu_4N)_2$[**5a**]), and $(Bu_4N)_2$[*cis*-$\{Re_6S_8Cl_4(bpy)_2\}$] ($(Bu_4N)_2$[**5b**]) were prepared according to the literatures.[27,63] Acetonitrile for electrochemical measurements was dried over calcium hydride and distilled under N_2 atmosphere. Non-luminescence grade acetonitrile (DOJIN) for spectroscopic measurements was used as received. Tetra-*n*-butylammonium hexafluorophosphate (Bu_4NPF_6) was prepared by metathesis of NH_4PF_6 with Bu_4NBr in water and recrystallized twice from ethanol. All other commercially available reagents were used as received.

Preparation of the Complexes (Bu_4N)[*mer*-$\{Re_6S_8Cl_3(ppy)_3\}$] ((Bu_4N)[1]), $(Bu_4N)_2$[*trans*-$\{Re_6S_8Cl_4(ppy)_2\}$] ($(Bu_4N)_2$[2a]), and $(Bu_4N)_2$[*cis*-$\{Re_6S_8Cl_4(ppy)_2\}$] ($(Bu_4N)_2$[2b]). A DMF solution (40 mL) of $(Bu_4N)_3[Re_6S_8Cl_6]$ (0.30 g, 0.13 mmol) and ppy (0.20 g, 1.30 mmol) was refluxed for 45 min, and the mixture was evaporated to dryness under reduced pressure. On the addition of 20 mL of benzene, a yellow-orange solid was deposited, which was collected by filtration. The solid was dissolved in dichloromethane, and the solution was chromatographed on a silica gel column. The first band eluted with dichloromethane/acetonitrile = 20/1 (v/v) was discarded. The second yellow-orange band eluted by dichloromethane/acetonitrile = 10/1 (v/v) was collected, and the eluate was allowed to stand until it became dryness. The residue was washed successively with water and diethyl ether, and then dried in air. Yield of (Bu_4N)[**1**]: 0.027 g (10%). Anal. Calcd for $C_{49}H_{63}N_4Cl_3Re_6S_8 \cdot 3H_2O$: C, 26.25; H, 3.10; N, 2.50. Found: C, 26.08; H, 2.84; N, 2.55. ^{1}H NMR (δ/ppm in DMSO-d_6): 0.93 (t, 12H, Bu_4N), 1.29 (m, 8H, Bu_4N), 1.56 (m, 8H, Bu_4N), 3.15 (m, 8H, Bu_4N), 7.57 (m, 9H, phenyl in ppy), 7.89 (m, 12H, H_m and phenyl in ppy), 9.34 (d, 4H, H_o), 9.41 (d, 2H, H_o). UV−vis absorption spectrum (nm (ε/M^{-1} cm^{-1}) in DMSO): 283 (73300).

The third yellow-orange band eluted by dichloromethane/acetonitrile = 10/1 (v/v) was collected, and the eluate was left for evaporation in air to dryness. The yellow-orange solid was washed successively with water and diethyl ether, and then dried in air. Yield of $(Bu_4N)_2$[**2a**]: 0.063 g (25%). Anal. Calcd for $C_{54}H_{90}N_4S_8Cl_2Re_6$: C, 28.07; H, 3.93; N, 2.42. Found: C, 27.94; H, 3.94; N, 2.63. ^{1}H NMR (δ/ppm in DMSO-d_6): 0.93 (t, 24H, Bu_4N), 1.29 (m, 16H, Bu_4N), 1.56 (m, 16H, Bu_4N), 3.15 (m, 16H, Bu_4N), 7.56 (m, 6H, phenyl in ppy), 7.85 (m, 8H, H_m and phenyl in ppy), 9.20 (d, 4H, H_o). UV−vis absorption spectrum (nm (ε/M^{-1} cm^{-1}) in CH_3CN): 317 (sh, 27500), 276 (63300), 221 (sh, 62400).

The fourth yellow-orange band eluted by dichloromethane/acetonitrile = 10/1 (v/v) was collected, and the eluate was left for evaporation in air to dryness. The yellow-orange solid was washed successively with water and diethyl ether, and then dried in air. Yield of $(Bu_4N)_2$[**2b**]: 0.086 g (34%). Anal. Calcd for $C_{54}H_{90}N_4S_8Cl_2Re_6$: C, 28.07; H, 3.93; N, 2.42. Found: C, 28.04; H, 3.94; N, 2.39. ^{1}H NMR (δ/ppm in DMSO-d_6): 0.93 (t, 24H, Bu_4N), 1.29 (m, 16H, Bu_4N), 1.56 (m, 16H, Bu_4N), 3.15 (m, 16H, Bu_4N), 7.57 (m, 6H, phenyl in ppy), 7.85 (m, 8H, H_m and phenyl in ppy), 9.35 (d, 4H, H_o). UV−vis absorption spectrum (nm (ε/M^{-1} cm^{-1}) in CH_3CN): 311 (sh, 29600), 274 (59400), 243 (sh, 42300), 223 (sh, 59300).

$(Bu_4N)_2$[*trans*-$\{Re_6S_8Cl_4(bpe)_2\}$] ($(Bu_4N)_2$[3a]) and $(Bu_4N)_2$-[*cis*-$\{Re_6S_8Cl_4(bpe)_2\}$] ($(Bu_4N)_2$[3b]). A DMF solution (95 mL) of $(Bu_4N)_3[Re_6S_8Cl_6]$ (0.700 g, 0.303 mmol) and bpe (0.557 g, 3.03 mmol) was heated at the reflux temperature for 25 min, and the mixture was evaporated to dryness under reduced pressure. On the addition of 70 mL of benzene, a yellow-orange solid was deposited, which was collected by filtration. The solid was dissolved in a minimum amount of dichloromethane, and the solution was chromatographed on a silica gel column. The first band eluted with dichloromethane/ethanol = 20/1 (v/v) was discarded. The second yellow-orange band eluted by dichloromethane/acetonitrile = 20/1 (v/v) was collected, and the eluate was left for evaporation in air to dryness. Yield of $(Bu_4N)_2$[**3a**]: 0.081 g (11%). Anal. Calcd for $C_{56}H_{96}N_6Cl_4Re_6S_8 \cdot 0.5CH_3CN$: C, 28.65; H, 4.11; N, 3.81. Found: C, 28.92; H, 4.05; N, 3.67. ^{1}H NMR (δ/ppm in CD_3CN): 0.96 (t, 24H, Bu_4N), 1.35 (m, 16H, Bu_4N), 1.59 (m, 16H, Bu_4N), 3.05 (m, 8H, $-CH_2-$), 3.08 (m, 16H, Bu_4N), 7.20 (m, 8H, H_m), 8.44 (d, 4H, H_o), 9.20 (d, 4H, H_o). UV−vis absorption spectrum (nm (ε/M^{-1} cm^{-1}) in CH_3CN): 428 (sh, 1300), 267 (sh, 33100), 240 (sh, 50300), 224 (76000).

The third yellow-orange band eluted by dichloromethane/acetonitrile = 20/1 (v/v) was collected, and the eluate was left for evaporation in air to dryness. Yield of $(Bu_4N)_2$[**3b**]: 0.148 g (20%). Anal. Calcd for $C_{56}H_{96}N_6Cl_4Re_6S_8$: C, 28.39; H, 4.09; N, 3.55. Found: C, 28.22; H, 4.07; N, 3.47. ^{1}H NMR (δ/ppm in CD_3CN): 0.96 (t, 24H, Bu_4N), 1.35 (m, 16H, Bu_4N), 1.59 (m, 16H, Bu_4N), 3.05 (m, 8H, $-CH_2-$), 3.07 (m, 16H, Bu_4N), 7.19 (m, 8H, H_m), 8.44 (d, 4H, H_o), 9.25 (d, 4H, H_o). UV−vis absorption spectrum (nm (ε/M^{-1} cm^{-1}) in CH_3CN): 426 (1100), 271 (sh, 25700), 243 (sh, 42000), 224 (63000).

Physical Measurements. ^{1}H NMR spectra were recorded on a 270.05 MHz JEOL JNM-EX 270 spectrometer. All peaks were referred to the residual methyl signals of acetonitrile at δ = 1.93 or DMSO at δ = 2.49. Cyclic voltammetry was performed using a Hokuto Denko HABF 1510 m potentiostat and a Graphtec WX4301 X-Y recorder. The working and counter electrodes comprised a glassy carbon disk and a platinum wire, respectively. Cyclic voltammograms were recorded at a scan rate of 100 mV/s. Sample solutions (ca. 1 mM) in 0.1 M Bu_4NPF_6-acetonitrile were deoxygenated by purging an N_2 gas stream.

(63) Long, J. R.; McCarty, L. S.; Holm, R. H. *J. Am. Chem. Soc.* **1996**, *118*, 4603–4616.

The reference electrode used was an Ag/AgCl electrode, against which the half-wave potential of a ferrocenium ion/ferrocene couple (Fc^+/Fc) was +0.43 V. UV−vis absorption spectra were recorded on a JASCO V-550 spectrophotometer. For photophysical measurements, sample solids were placed between two nonfluorescent glass plates, and solution samples were deoxygenated by purging an Ar gas stream for at least 15 min and then sealed. For spectroscopic and photophysical experiments at 80 K, the temperature (±0.1 K) was controlled by using a liquid-N_2 cryostat system (Oxford Instruments). A pulsed Nd^{3+}:YAG laser (Continuum Surelite, 355 nm, fwhm ~6 ns) was used as an exciting light source. Corrected emission spectra were recorded on a red-sensitive multichannel photodetector (Hamamatsu Photonics, PMA-11), and the emission lifetime was measured by using a streak camera (Hamamatsu Photonics, C4334). Emission quantum yields were estimated by using $(Bu_4N)_4[Re_6S_8Cl_6]$ (Φ_{em} = 0.039) in acetonitrile as a standard.

X-ray Structural Determination. Single crystals of $(Bu_4N)_2$-[**2a**] and $(Bu_4N)_2$[**3a**] suitable for X-ray analysis were obtained by recrystallization from the acetonitrile/diethyl ether and acetonitrile/toluene solutions, respectively. X-ray data of both $(Bu_4N)_2$[**2a**] and $(Bu_4N)_2$[**3a**] were collected at −103 °C on a Rigaku RAXIS RAPID diffractometer with graphite monochromated Mo *K*α radiation. The crystal structures were solved by the Patterson method (DIRDIF94) or direct method (SIR92). Atomic coordinates and thermal parameters of nonhydrogen atoms were calculated by a full-matrix least-squares method. The hydrogen atoms except for those of Bu_4N^+ in $(Bu_4N)_2$[**3a**] were placed at the calculated positions by using the riding model. The carbon atom (C25) of Bu_4N^+ in $(Bu_4N)_2$[**3a**] was found to be disordered over two sites with a 0.5:0.5 occupancy. Calculations were performed using a TEXSAN software package.[64] The crystallographic data are listed in Table 1.

Computational Methods. All the MO calculations were performed with the Gaussian 03 program at the B3LYP[65−67] level using Lanl2dz basis set.[68] The single-point density-functional theory (DFT) and time-dependent DFT (TD-DFT) calculations with self-consistent reaction field models (solvent = acetonitrile) were performed for $[Re_6S_8Cl_6]^{4-}$, *trans*-$[Re_6S_8Cl_4(ppy)_2]^{2-}$, and *trans*-$[Re_6S_8Cl_4(bpy)_2]^{2-}$. The calculations were performed using the structures of the complexes determined by a single-crystal X-ray analysis except in the case of *trans*-$[Re_6S_8Cl_4(bpy)_2]^{2-}$. Since the X-ray structure of *trans*-$[Re_6S_8Cl_4(bpy)_2]^{2-}$ was not available, we performed the calculations based on the structure of *trans*-$[Re_6S_8Cl_4(ppy)_2]^{2-}$ by substituting ppy groups with bpy. The atomic parameters used for the calculations of *trans*-$[Re_6S_8Cl_4(bpy)_2]^{2-}$ are shown in Supporting Information, Table S1. The energies and components of MOs near the frontier orbital levels for *trans*-$[Re_6S_8Cl_4(ppy)_2]^{2-}$ and *trans*-$[Re_6S_8Cl_4(bpy)_2]^{2-}$ were calculated as given in the data in Supporting Information, Tables S2 and S3, respectively. The energy, oscillator strength, and calculated transitions for *trans*-$[Re_6S_8Cl_4(ppy)_2]^{2-}$ and *trans*-$[Re_6S_8Cl_4(bpy)_2]^{2-}$ are summarized in the Supporting Information, Tables S4 and S5, respectively.

Table 1. Crystallographic Data for $(Bu_4N)_2$[*trans*-$\{Re_6S_8Cl_4(ppy)_2\}$] ($(Bu_4N)_2$-[**2a**]) and $(Bu_4N)_2$[*trans*-$\{Re_6S_8Cl_4(bpe)_2\}$] ($(Bu_4N)_2$[**3a**])

	$(Bu_4N)_2$[**2a**]	$(Bu_4N)_2$[**3a**]
formula	$C_{54}H_{90}N_4Cl_4Re_6S_8$	$C_{56}H_{96}N_6Cl_4Re_6S_8$
Fw	2310.87	2368.95
crystal system	monoclinic	monoclinic
space group	$P2_1/n$	$P2_1/c$
a/Å	13.087(4)	13.520(6)
b/Å	16.822(6)	10.835(4)
c/Å	15.229(5)	23.838(3)
β/deg	98.54(1)	92.78(1)
V/Å^3	3315(2)	3488(2)
D/g cm^{-3}	2.315	2.255
T/K	170.2	170.2
μ/cm^{-1}	11.365	10.807
$R1$	0.0238	0.0366
Rw	0.0456	0.0821
GOF	1.083	1.023

$R1 = \sum||F_o| - |F_c||/\sum|F_o|$; $Rw = [\sum w(F_o^2 - F_c^2)^2/\sum w(F_o^2)^2]^{1/2}$.

Results and Discussion

Preparation of the Complexes. Hexarhenium complexes containing terminal ppy or bpe ligands were prepared by the reaction of $[Re_6S_8Cl_6]^{3-}$ with ppy or bpe in a molar ratio of 1:10 in DMF at the reflux temperature. The products were separated by column chromatography using dichloromethane/acetonitrile or dichloromethane/ethanol as the eluent for the ppy or bpe complexes, respectively. The ^{1}H NMR spectra in the chemical shift region of the pyridyl and phenyl moieties are shown in Supporting Information, Figure S1. The complexes having bis- and tris-N-heteroaromatic ligands were discriminated by using the integrated intensity ratio of the proton signals of the Bu_4N^+ cations to those of the coordinated pyridyl ligands. In the column chromatographic separation of the ppy complexes, the tris(ppy) complex was eluted first. The ^{1}H NMR spectrum of the tris(ppy) complex showed two sets of the ligand signals in a 2:1 integrated intensity ratio, indicating that the complex possessed a meridional geometry. In the case of the bis(ppy) and bis(bpe) complexes, the band that eluted first in column chromatography was assigned to the trans isomer on the basis of the experimental findings described below. The trans isomer of $[Re_6S_8Cl_4L_2]^{2-}$ (L = 4-dimethylaminopyridine (dmap), mpy, py, bpy, 4-cyanopyridine (cpy), or pz) was always eluted first in the column chromatography, and this was followed by the corresponding cis isomer.[27,28] Second, only one set of the ligand signals could be observed for each complex in the ^{1}H NMR spectrum. Third, the ortho proton signals of the pyridine derivatives in the trans isomer appear at higher magnetic fields than in the case of the cis isomer. These conclusions are consistent with the results from the X-ray analysis of $(Bu_4N)_2$[**2a**] and $(Bu_4N)_2$[**3a**] (vide infra).

X-ray Crystal Structures of $(Bu_4N)_2$[2a] and $(Bu_4N)_2$-[3a]. The Oak Ridge Thermal-Ellipsoid Plot (ORTEP) drawings of the complex anions of $(Bu_4N)_2$[**2a**] and

(64) *TEXSAN*; Molecular Structure Corp.: The Woodlands, TX, 1985 and 1992.
(65) Becke, A. D. *J. Chem. Phys.* **1993**, *98*, 5648–5652.
(66) Becke, A. D. *Phys. Rev. B* **1988**, *38*, 3098–3100.
(67) Lee, C.; Yang, W.; Parr, R. G. *Phys. Rev. B* **1988**, *37*, 785–789.
(68) Frisch, M. J.; Trucks, G. W.; Schlegel, H. B.; Scuseria, G. E.; Robb, M. A.; Cheeseman, J. R.; Montgomery, J., J. A.; Vreven, T.; Kudin, K. N.; Burant, J. C.; Millam, J. M.; Iyengar, S. S.; Tomasi, J.; Barone, V.; Mennucci, B.; Cossi, M.; Scalmani, G.; Rega, N.; Petersson, G. A.; Nakatsuji, H.; Hada, M.; Ehara, M.; Toyota, K.; Fukuda, R.; Hasegawa, J.; Ishida, M.; Nakajima, T.; Honda, Y.; Kitao, O.; Nakai, H.; Klene, M.; Li, X.; Knox, J. E.; Hratchian, H. P.; Cross, J. B.; Bakken, V.; Adamo, C.; Jaramillo, J.; Gomperts, R.; Stratmann, R. E.; Yazyev, O.; Austin, A. J.; Cammi, R.; Pomelli, C.; Ochterski, J. W.; Ayala, P. Y.; Morokuma, K.; Voth, G. A.; Salvador, P.; Dannenberg, J. J.; Zakrzewski, V. G.; Dapprich, S.; Daniels, A. D.; Strain, M. C.; Farkas, O.; Malick, D. K.; Rabuck, A. D.; Raghavachari, K.; Foresman, J. B.; Ortiz, J. V.; Cui, Q.; Baboul, A. G.; Clifford, S.; Cioslowski, J.; Stefanov, B. B.; Liu, G.; Liashenko, A.; Piskorz, P.; Komaromi, I.; Martin, R. L.; Fox, D. J.; Keith, T.; Al-Laham, M. A.; Peng, C. Y.; Nanayakkara, A.; Challacombe, M.; Gill, P. M. W.; Johnson, B.; Chen, W.; Wong, M. W.; Gonzalez, C.; Pople, J. A.; *Gaussian 03*, Revision C.02; Gaussian, Inc.: Wallingford, CT, 2004.

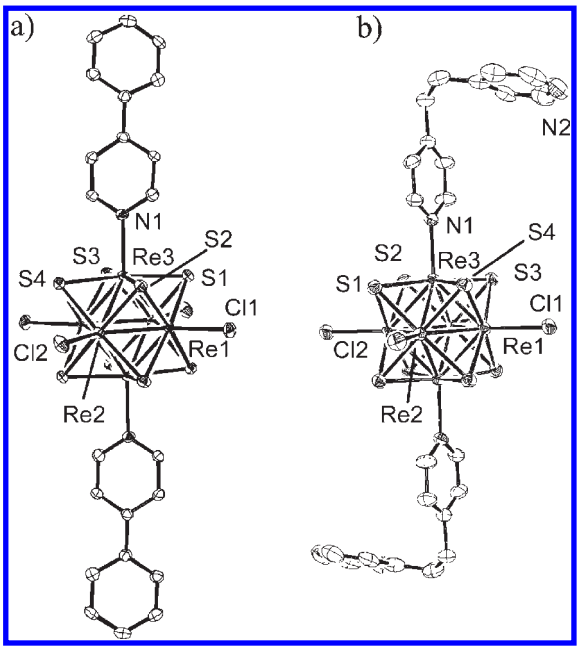

Figure 1. ORTEP drawings showing the complex anion and numbering scheme for (a) $(Bu_4N)_2$[*trans*-$\{Re_6S_8Cl_4(ppy)_2\}$] ($(Bu_4N)_2$[**2a**]) and (b) $(Bu_4N)_2$[*trans*-$\{Re_6S_8Cl_4(bpe)_2\}$] ($(Bu_4N)_2$[**3a**]). Ellipsoids are drawn at the 50% probability level. The hydrogen atoms have been omitted for clarity.

Table 2. Selected Bond Distances (Å) and Angles (deg) for $(Bu_4N)_2$[*trans*-$\{Re_6S_8Cl_4(ppy)_2\}$] ($(Bu_4N)_2$[**2a**]) and $(Bu_4N)_2$[*trans*-$\{Re_6S_8Cl_4(bpe)_2\}$] ($(Bu_4N)_2$[**3a**])

	$(Bu_4N)_2$[**2a**]	$(Bu_4N)_2$[**3a**]
Re−Re	2.592(1)−2.605(1) av.2.598(1)	2.5919(7)−2.6041(9) av.2.596(1)
Re−S	2.404(1)−2.416(1) av.2.410(3)	2.398(2)−2.415(2) av.2.407(7)
Re−Cl	2.435(1)	2.430(2)
Re−N	2.216(3)	2.198(5)
Re−Re−Re	59.790(6)−60.310(7) av.60.00(3)	59.80(1)−60.28(2) av.60.00(5)
Re−Re−Re	89.582(7)−90.418(7) av. 90.00(7)	89.63(1)−90.37(1) av.90.00(4)
Re−S−Re	65.08(3)−65.52(3) av.65.2(1)	65.01(4)−65.61(5) av.65.3(2)
S−Re−S	89.42(4)−90.02(4) av.89.8(1)	89.28(6)−90.34(6) av.89.8(2)
S−Re−S	173.18(4)−174.20(3) av.173.56(8)	173.03(6)−174.37(6) av.173.5(1)
Re−Re−N	132.25(9)−137.32(9) av.134.8(2)	134.5(1)−135.1(1) av.134.8(2)
Re−Re−Cl	133.12(3)−137.25(3) av.135.08(8)	133.57(4)−136.78(4) av.135.1(1)

$(Bu_4N)_2$[**3a**] are shown in Figure 1. The two pyridyl type ligands were coordinated at mutually trans terminal sites of the Re_6S_8 core with the chloride ligands coordinated at the other terminal sites. The selected bond distances and angles are listed in Table 2. The six rhenium atoms form a nearly regular octahedron with the Re−Re distances of 2.592(1)−2.605(1) Å for $(Bu_4N)_2$[**2a**] and 2.5919(7)−2.6041(9) Å for $(Bu_4N)_2$[**3a**]. The Re−S and Re−Cl distances in $(Bu_4N)_2$[**2a**] were 2.404(1)−2.416(1) and 2.435(1) Å, respectively, and the corresponding values in $(Bu_4N)_2$[**3a**] were 2.398(2)−2.415(2) and 2.430(2) Å, respectively. These distances are almost comparable to those of other hexarhenium complexes. The Re−N bond distances of 2.216(3) and 2.198(5) Å for $(Bu_4N)_2$[**2a**] and $(Bu_4N)_2$[**3a**], respectively, were similar to those of *trans*-$[Re_6S_8Cl_4L_2]^{2-}$ (L = py, cpy, or pz),[27,28] $[Re_6Se_8(PEt_3)_nL_{6-n}]^{2+}$ (L = bpy, n = 4, 5; L = isonicotinamide, n = 4, 5; L = 3,5-pyridinedicarboxylic acid, n = 4, 5),[18,19,29] $[\{Re_6Se_8(PEt_3)_5\}_2L]^{4+}$ (L = bpy, bpe),[18] $[\{Re_6Se_8(PPh_3)_4(bpy)_2\}_2\{Cd(NO_3)_2\}]^{4+}$, and $[\{Re_6Se_8(PPh_3)_4(bpy)_2\}\{M(NO_3)_3\}]^{+}$ (M = Cd, Co, Zn).[30,31]

Electrochemistry. Cyclic voltammograms (CVs) of $[$**2a,b**$]^{2-}$ and $[$**3a,b**$]^{2-}$ were measured in 0.1 M Bu_4NPF_6-acetonitrile solutions (the abbreviation $[$**2a,b**$]^{2-}$ is used when two complexes, $[$**2a**$]^{2-}$ and $[$**2b**$]^{2-}$, are discussed simultaneously. The terminologies $[$**3a,b**$]^{2-}$ and $[$**5a,b**$]^{2-}$ are also used similarly.). Figures S2, S3, and S4 in Supporting Information show the CVs of $[$**1**$]^{-}$ and $[$**4**$]^{-}$, $[$**2a,b**$]^{2-}$, and $[$**3a,b**$]^{2-}$, respectively. Table 3 summarizes the redox potentials of these complexes along with those of the bpy and pz complexes $[Re_6S_8Cl_{6-n}L_n]^{n-4}$ (L = bpy, pz). The redox potentials of $[$**1**$]^{-}$ and $[$**4**$]^{-}$ were determined in Bu_4NPF_6-DMSO solutions because of their low solubilities in Bu_4NPF_6-acetonitrile. Reversible one-electron oxidation waves assigned to the $Re(III)_6/Re(III)_5Re(IV)$ process were observed at identical potentials for the two isomers: +0.77 V for $[$**2a,b**$]^{2-}$ and +0.76 V for $[$**3a,b**$]^{2-}$. The ppy complexes $[$**2a,b**$]^{2-}$ exhibited two-electron reduction waves at around −1.7 V. These waves could be assigned to the ligand-centered reduction processes, as observed in the case of the bis(bpy) and bis(pz) complexes. These results indicate that LUMOs of the ppy complexes $[$**1**$]^{-}$ and $[$**2a,b**$]^{2-}$ are ligand-centered similar to those of the bis(bpy), bis(pz), and bis(cpy) complexes.[27] The bpe complexes $[$**3a,b**$]^{2-}$ did not show any reduction wave up to −1.8 V. This is readily understood since the reduction of the bpe ligand proceeds at a more negative potential than that of ppy. Although the dependence of the redox potentials of the $Re(III)_6/Re(III)_5Re(IV)$ process on the type of terminal ligand and ligand−ligand redox interactions are very important for the chemistry of a hexarhenium(III) complex, this is not the primary issue of the present study in this paper; we focus on the discussions on the ground-state highest occupied MO (HOMO)-LUMO levels of the hexarhenium(III) complexes in relation to their spectroscopic and photophysical properties. Therefore, we have reported detailed discussion of the redox properties of the new complexes in the Supporting Information.

Spectroscopic and Excited-State Properties. (1). Emission Spectra in Solution and Solid Phases. Emission spectroscopy and photophysical measurements for the hexarhenium(III) complexes were conducted in acetonitrile at 298 K and in the solid phase at 80 and 298 K. As a typical example, the emission spectra of $[$**1**$]^{-}$, $[$**2a,b**$]^{2-}$, and $[$**4**$]^{-}$ in acetonitrile at 298 K are shown in Figure 2, and those in the solid phases at 80 and 298 K are shown in Figure 3. The emission spectra of $[$**3a,b**$]^{2-}$ in acetonitrile at 298 K are shown in Supporting Information, Figure S5. The emission spectra of $[$**5a,b**$]^{2-}$ in the solid states at 80 and 298 K are shown in Figure 4. The spectroscopic (emission maximum wavelength (λ_{em})) and photophysical parameters (emission quantum yield (Φ_{em}) and lifetime (τ_{em})) of the complexes are summarized in Table 4.

We have previously reported the emission data (λ_{em}, Φ_{em}, and τ_{em}) of *trans*/*cis*-$[Re_6S_8Cl_4L_2]^{2-}$ (L = py, mpy, bpy, and pz) and *mer*-$[Re_6S_8Cl_3(py)_3]^{-}$ in acetonitrile at

Table 3. Redox Potentials and ΔE_{redox} for $(Bu_4N)_{4-n}[Re_6S_8Cl_{6-n}L_n]$ (L = ppy, n = 2, 3; L = bpe, n = 2; L = bpy, n = 2, 3; L = pz, n = 2) in 0.1 M Bu_4NPF_6-Acetonitrile

	$E_{1/2}$/V vs Ag/AgCl		
	$Re(III)_6/Re(III)_5Re(IV)$	$L^{\cdot-}/L$	ΔE_{redox}[a]
(Bu_4N)[*mer*-$\{Re_6S_8Cl_3(ppy)_3\}$][b] ((Bu_4N)[**1**])	+1.01	−1.57[c], −1.78[c,d]	+2.58
$(Bu_4N)_2$[*trans*-$\{Re_6S_8Cl_4(ppy)_2\}$] ($(Bu_4N)_2$[**2a**])	+0.77	−1.70[c]	+2.47
$(Bu_4N)_2$[*cis*-$\{Re_6S_8Cl_4(ppy)_2\}$] ($(Bu_4N)_2$[**2b**])	+0.77	−1.65, −1.74	+2.42
$(Bu_4N)_2$[*trans*-$\{Re_6S_8Cl_4(bpe)_2\}$] ($(Bu_4N)_2$[**3a**])	+0.76		
$(Bu_4N)_2$[*cis*-$\{Re_6S_8Cl_4(bpe)_2\}$] ($(Bu_4N)_2$[**3b**])	+0.76		
(Bu_4N)[*mer*-$\{Re_6S_8Cl_3(bpy)_3\}$][b] ((Bu_4N)[**4**])	+1.06	−1.20[c], −1.49[c,d]	+2.26
$(Bu_4N)_2$[*trans*-$\{Re_6S_8Cl_4(bpy)_2\}$][e] ($(Bu_4N)_2$[**5a**])	+0.79	−1.45[d]	+2.24
$(Bu_4N)_2$[*cis*-$\{Re_6S_8Cl_4(bpy)_2\}$][e] ($(Bu_4N)_2$[**5b**])	+0.79	−1.44[d]	+2.23
$(Bu_4N)_2$[*trans*-$\{Re_6S_8Cl_4(pz)_2\}$][e] ($(Bu_4N)_2$[**6a**])	+0.86	−1.34, −1.45	+2.20
$(Bu_4N)_2$[*cis*-$\{Re_6S_8Cl_4(pz)_2\}$][e] ($(Bu_4N)_2$[**6b**])	+0.86	−1.33, −1.47	+2.19

[a] $\Delta E_{redox} = E_{1/2}(Re(III)_6/Re(III)_5Re(IV)) - E_{1/2}(L^{\cdot-}/L$(the first process)). [b] In 0.1 M Bu_4NPF_6-DMSO. [c] E_{pc} value. [d] Two-electron process. [e] Ref 27.

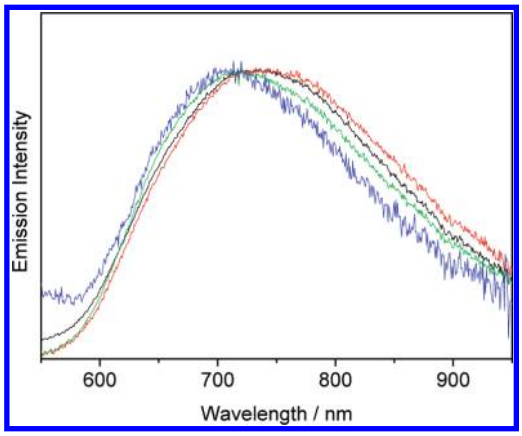

Figure 2. Emission spectra for (Bu_4N)[*mer*-$\{Re_6S_8Cl_3(ppy)_3\}$] ((Bu_4N)[**1**]) (black), $(Bu_4N)_2$[*trans*-$\{Re_6S_8Cl_4(ppy)_2\}$] ($(Bu_4N)_2$[**2a**]) (red), $(Bu_4N)_2$[*cis*-$\{Re_6S_8Cl_4(ppy)_2\}$] ($(Bu_4N)_2$[**2b**]) (green), and (Bu_4N)[*mer*-$\{Re_6S_8Cl_3(bpy)_3\}$] ((Bu_4N)[**4**]) (blue) at 298 K in acetonitrile.

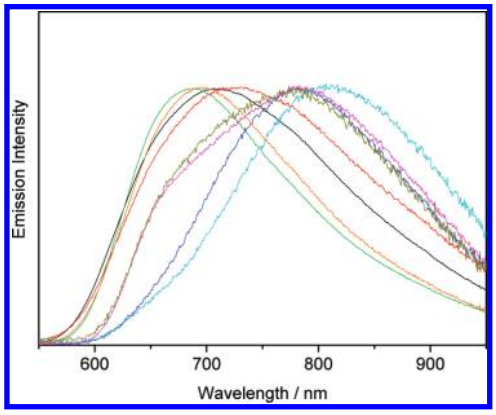

Figure 3. Emission spectra for (Bu_4N)[*mer*-$\{Re_6S_8Cl_3(ppy)_3\}$] ((Bu_4N)[**1**]) at 298 (black) and 80 K (blue), $(Bu_4N)_2$[*trans*-$\{Re_6S_8Cl_4(ppy)_2\}$] ($(Bu_4N)_2$[**2a**]) at 298 (red) and 80 K (sky blue), $(Bu_4N)_2$[*cis*-$\{Re_6S_8Cl_4(ppy)_2\}$] ($(Bu_4N)_2$[**2b**]) at 298 (green) and 80 K (purple), and (Bu_4N)[*mer*-$\{Re_6S_8Cl_3(bpy)_3\}$] ((Bu_4N)[**4**]) at 298 (orange) and 80 K (dark yellow) in the solid state.

298 K, and demonstrated that the complexes could be classified into two groups. One (group A) comprises the complexes with py and mpy ligands, while the other group (group B) comprises those with bpy and pz ligands having a free nitrogen end.[27] The group A complexes show photophysical characteristics (λ_{em} = 740−750 nm, Φ_{em} = 0.031−0.057, and τ_{em} = 4.2−6.2 μs) similar to those of $[Re_6S_8X_6]^{4-}$ (X = Cl, Br, or I) (λ_{em} = 770−800 nm,

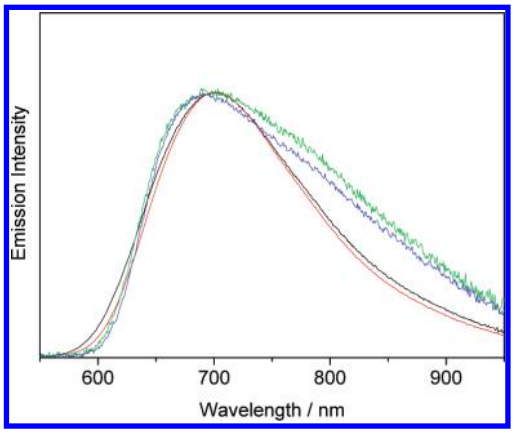

Figure 4. Emission spectra for $(Bu_4N)_2$[*trans*-$\{Re_6S_8Cl_4(bpy)_2\}$] ($(Bu_4N)_2$[**5a**]) at 298 (black) and 80 K (green), and $(Bu_4N)_2$-[*cis*-$\{Re_6S_8Cl_4(bpy)_2\}$] ($(Bu_4N)_2$[**5b**]) at 298 (red) and 80 K (blue) in the solid state.

Φ_{em} = 0.015−0.039, and τ_{em} = 4.4−6.3 μs), although the emission spectra of $[Re_6S_8Cl_4L_2]^{2-}$ (L = py or mpy) is shifted to a shorter wavelength relative to those of $[Re_6S_8Cl_6]^{4-}$. In the case of the group B complexes (λ_{em} = 763−785 nm, Φ_{em} = 0.0010−0.0017, and τ_{em} = 0.013−0.029 μs), although the emission maximum wavelengths are close to those of the hexa-halogeno complexes, the Φ_{em} and τ_{em} values are smaller and shorter, respectively, by a few orders of magnitude as compared with the relevant value of $[Re_6S_8Cl_6]^{4-}$. On the basis of these data, it was suggested that the emissive excited states of the latter complexes might have a MLCT character.[27] It should be noted that the complexes $[\mathbf{5a,b}]^{2-}$, which are the target of the present detailed study, are included in group B.

The complexes $[\mathbf{1}]^-$, $[\mathbf{2a,b}]^{2-}$, $[\mathbf{3a,b}]^{2-}$, and $[\mathbf{4}]^-$ in acetonitrile at 298 K exhibited broad and structureless emission with λ_{em} = 709−751 nm, Φ_{em} = 0.0057−0.042, and τ_{em} = 1.01−5.88 μs. These data indicate that all of these complexes can be classified into group A, because of the similarities of the λ_{em}, Φ_{em}, and τ_{em} values with those of $[Re_6S_8Cl_4L_2]^{2-}$ with py or mpy. It is noteworthy that despite the presence of free nitrogen sites, the bis(bpe) complexes $[\mathbf{3a,b}]^{2-}$ are included in this group. Namely, all the complexes exhibit emissions similar to the Re_6S_8 core-center type emission. Furthermore, it is interesting to note that the photophysical data of $[\mathbf{4}]^-$ (λ_{em} = 709 nm, Φ_{em} = 0.0057, and τ_{em} = 1.01 μs) are significantly different from those of $[\mathbf{5a,b}]^{2-}$ (classified into group B), despite the

Table 4. Photophysical Data for $(Bu_4N)_{4-n}[Re_6S_8Cl_{6-n}L_n]$ (L = ppy, n = 2, 3; L = bpe, n = 2; L = bpy, n = 2, 3; L = pz, n = 2) in Acetonitrile at 298 K and in the Solid State at 298 and 80 K

	CH_3CN			solid state			
	298 K			298 K		80 K	
	λ_{em}/ nm	Φ_{em}	$\tau_{em}/\mu s$	λ_{em}/ nm	$\tau_{em}/\mu s$	λ_{em}/ nm	$\tau_{em}/\mu s$
(Bu_4N)[*mer*-$\{Re_6S_8Cl_3(ppy)_3\}$] ((Bu_4N)[**1**])	728	0.042	5.74	705	1.73, 5.30	784	4.32, 21.16
$(Bu_4N)_2$[*trans*-$\{Re_6S_8Cl_4(ppy)_2\}$] ($(Bu_4N)_2$[**2a**])	734	0.030	4.09	727	2.03, 4.09	653, 804	5.64, 17.50
$(Bu_4N)_2$[*cis*-$\{Re_6S_8Cl_4(ppy)_2\}$] ($(Bu_4N)_2$[**2b**])	720	0.038	4.09	685	4.91	655, 782	5.21, 18.79
$(Bu_4N)_2$[*trans*-$\{Re_6S_8Cl_4(bpe)_2\}$] ($(Bu_4N)_2$[**3a**])	751	0.024	4.40	738	0.78, 3.99	648, 830	14.22[b]
$(Bu_4N)_2$[*cis*-$\{Re_6S_8Cl_4(bpe)_2\}$] ($(Bu_4N)_2$[**3b**])	746	0.036	5.88	718	0.81, 4.47	650, 795	3.30, 15.78
(Bu_4N)[*mer*-$\{Re_6S_8Cl_3(bpy)_3\}$] ((Bu_4N)[**4**])	709	0.0057	1.01	696	0.95, 3.12	656, 775	17.51[b]
$(Bu_4N)_2$[*trans*-$\{Re_6S_8Cl_4(bpy)_2\}$] ($(Bu_4N)_2$[**5a**])	763[a]	0.0013[a]	0.019[a]	699	2.92[b]	694	3.35, 14.38
$(Bu_4N)_2$[*cis*-$\{Re_6S_8Cl_4(bpy)_2\}$] ($(Bu_4N)_2$[**5b**])	768[a]	0.0011[a]	0.013[a]	701	0.50, 1.91	689	14.77[b]
$(Bu_4N)_2$[*trans*-$\{Re_6S_8Cl_4(pz)_2\}$] ($(Bu_4N)_2$[**6a**])	782[a]	0.0017[a]	0.029,0.013[a]				
$(Bu_4N)_2$[*cis*-$\{Re_6S_8Cl_4(pz)_2\}$] ($(Bu_4N)_2$[**6b**])	785[a]	0.0010[a]	0.021[a]				

[a] Ref 27. [b] The data cannot fit double exponential decay. The longest lifetime value is shown.

fact that both $[\mathbf{4}]^-$ and $[\mathbf{5a,b}]^{2-}$ possess mixed-chloro-bpy terminal ligands. The difference in the photophysical data between $[\mathbf{2a,b}]^{2-}$ (bis(ppy)) and $[\mathbf{1}]^-$ (tris(ppy)) is less significant.

In the solid state at 80 and 298 K, the hexarhenium complexes exhibited broad and structureless emissions as seen in Figures 3 and 4. In the case of $[Re_6S_8Cl_6]^{4-}$, the emission maximum wavelength (λ_{em}) and the emission spectral band shape in the solid state agree almost completely with those in solution.[69] Gray et al. also reported the emission spectra of 14 hexarhenium(III) complexes in both CH_2Cl_2 and solid state, and the differences in the λ_{em} values between the two phases were small (<20 nm).[53] Such good correspondence between the emission characteristics of a hexarhenium(III) complex in the solid and solution phases is a common feature of the Re_6S_8 core-centered emission. However, the present hexarhenium(III) complexes show an appreciable shift in the emission maxima in the two phases, that is, those in the solid state at 298 K located at appreciably shorter wavelengths as compared to that of the corresponding complex in acetonitrile. Nevertheless, in the case of $[\mathbf{1}]^-$, $[\mathbf{2a,b}]^{2-}$, $[\mathbf{3a,b}]^{2-}$, and $[\mathbf{4}]^-$, the shift in the emission maximum wavelength can be considered to be rather mild; a shift to shorter wavelengths by 7−35 nm occurs when changing from the solid state to acetonitrile solution. In contrast to the rather mild shift for these complexes, the corresponding shift of the group B complexes $[\mathbf{5a}]^{2-}$ or $[\mathbf{5b}]^{2-}$ was as large as 64−67 nm; these should certainly be considered exceptional. In addition to this abnormality of $[\mathbf{5a}]^{2-}$ or $[\mathbf{5b}]^{2-}$, a close inspection of the data at 298 K indicates that the full-width at half-maximum (fwhm) values of the emission spectra of $[\mathbf{5a,b}]^{2-}$ in the solid state are considerably smaller (3100−3270 cm^{-1}) than those observed in the case of the other complexes: 3590−4640 cm^{-1}.

All these results clearly indicate that the photophysical properties of $[\mathbf{5a,b}]^{2-}$ that are classified into the group B are significantly different from those of the other hexarhenium(III) complexes whose emissions undoubtedly originate from the Re_6S_8 core. As discussed above, the photophysical properties of the group B complexes are characterized by significantly small quantum yields Φ_{em} and short lifetimes τ_{em}. It is noteworthy that the emission lifetimes of $[\mathbf{5a,b}]^{2-}$ at 298 K in the solid state are considerably longer (1.9−2.9 μs) than those in solution (0.013−0.019 μs), while the τ_{em} values of other hexarhenium complexes are very similar in both solution and solid state: see Table 4. Therefore, it is suggested that the emission pathway of $[\mathbf{5a,b}]^{2-}$ may be significantly influenced by a solvent; this is reminiscent of the behavior observed for the MLCT excited state of a polypyridine ruthenium(II) complex.

Large differences in the photophysical characteristics between $[\mathbf{5a,b}]^{2-}$ and other hexarhenium complexes were observed in the case of the low-temperature emission spectra in the solid phase as well. While the λ_{em} values of $[\mathbf{1}]^-$, $[\mathbf{2a,b}]^{2-}$, $[\mathbf{3a,b}]^{2-}$, and $[\mathbf{4}]^-$ were shifted to the longer wavelengths by 77−97 nm upon cooling from 298 to 80 K, those of $[\mathbf{5a,b}]^{2-}$ exhibited shorter-wavelength shifts. As reported previously by our research groups and Gray et al., the emission spectrum of a hexarhenium(III) complex represented by $[Re_6S_8X_6]^{4-}$ (X = Cl, Br, I) exhibits a longer wavelength shift upon cooling from room temperature to 80 K in both solid and glass phases.[47,53,55] The origin of the temperature (T)-dependent emission spectral shift could be the zero-field splitting of the degenerated emitting excited triplet state to spin sublevels as a result of the relatively large spin−orbit coupling experienced by the complex. At room temperature, the emission from the higher-energy lying spin-sublevel(s) contributes to the total emission spectrum, while that from the lower-energy lying spin-sublevel(s) participates in low-temperature emission, leading to a longer wavelength (lower-energy) shift in the emission upon cooling.[55] Therefore, the T-dependent emission shifts of $[\mathbf{5a,b}]^{2-}$ mentioned above cannot be explained in the same manner as that of $[Re_6S_8X_6]^{4-}$. The differences in the excited states of $[\mathbf{5a,b}]^{2-}$ and other hexarhenium complexes will be discussed in greater detail in the following section after the theoretical considerations are described.

Another notable feature of the solid state emission spectrum at 80 K is that $[\mathbf{2b}]^{2-}$ and $[\mathbf{4}]^-$ exhibit a distinct emission shoulder in the shorter wavelength region of the maximum wavelength. The contribution of the emission shoulder to the total spectrum is minor in the case of other

(69) Kitamura, N.; Yamada, K.; Ueda, Y.; Sasaki, Y.; Ishizaka, S., submitted for publication.

complexes. In the solid state, the excitation energy migration sometimes proceeds very efficiently, and the excitation energy is trapped at various crystal defect sites, which emit luminescence independently. In practice, these complexes exhibited non-single exponential decays even at 298 K, with the exception of $[\mathbf{2b}]^{2-}$. Therefore, we suppose that the emission shoulders and non-single exponential emission decays observed for these complexes would be due to the presence of crystal defects.

(2). DFT Calculations of the HOMO/LUMO Levels and Absorption Transitions. Theoretical studies on the HOMO/LUMO levels and the electronic transition energies in $[Re_6S_8X_6]^{4-}$ (X = Cl, Br, I, CN) have been hitherto conducted by several research groups.[53,54,59−62,70] Some of these reports demonstrate that the HOMO and lower-energy lying occupied MOs reside mainly in the Re_6S_8 core, while the LUMOs and higher-energy lying unoccupied MOs are characterized by more restricted metal orbitals in the Re_6S_8 core.[53,59,61] The substantially allowed lowest-energy absorption bands in these complexes have been thus ascribed to the transitions within the Re_6S_8 core.[61] We also conducted DFT calculations on the HOMO/LUMO levels and absorption transition energies in *trans*-$[Re_6S_8Cl_4L_2]^{2-}$ (L = ppy or bpy) at the Gaussian03 level.[71] Tables 5 and 6 summarize the energies and components in the vicinity of the HOMO/LUMO levels of *trans*-$[Re_6S_8Cl_4(ppy)_2]^{2-}$ ($[\mathbf{2a}]^{2-}$) and *trans*-$[Re_6S_8Cl_4(bpy)_2]^{2-}$ ($[\mathbf{5a}]^{2-}$), respectively. The contour plots of the MOs near the frontier orbital levels calculated for $[\mathbf{2a}]^{2-}$ and $[\mathbf{5a}]^{2-}$ are shown in the Supporting Information, Figures S6 and S7. For both $[\mathbf{2a}]^{2-}$ and $[\mathbf{5a}]^{2-}$, we found that the HOMO and HOMO−1 were characterized essentially in the orbitals of the Re_6S_8 core, similar to those of $[Re_6S_8X_6]^{4-}$. On the other hand, significant contributions from the ppy and bpy ligands were observed in the lower-energy lying unoccupied orbitals of $[\mathbf{2a}]^{2-}$ and $[\mathbf{5a}]^{2-}$, respectively, particularly in the bpy complex. While the LUMO and LUMO+2 levels of the bis(bpy) complex $[\mathbf{5a}]^{2-}$ have significant contributions from the bpy ligand (64 and 86%, respectively), the contributions from the ppy ligand in the bis(ppy) complex $[\mathbf{2a}]^{2-}$ to LUMO+1 and LUMO+2 are 48 and 72%, respectively. The lowest-energy unoccupied π^* orbital of the bpy ligand is located between the occupied and the unoccupied orbitals of the Re_6S_8 core in terms of energy. In the case of the bis(ppy) complex, the situation will be more delicate, and the ppy π^* and Re_6S_8 core-centered unoccupied orbitals would be located in close proximity in terms of energy.

Electronic transitions from the orbitals in the HOMO regions to those in the LUMO regions were also calculated. Our TD-DFT calculations on *trans*-$[Re_6S_8Cl_4(ppy)_2]^{2-}$ indicate that the substantially allowed lowest-energy absorption transitions can be ascribed to both Re_6S_8 core-to-ppy ligand CT (MLCT) and Re_6S_8 core-centered transitions: HOMO−1 → LUMO+2 (41%)/HOMO → LUMO+2 (27%) transitions with oscillator strength (*f*) of 0.0005 and HOMO → LUMO+2 (55%)/HOMO−1 → LUMO+2 (24%) transitions with $f = 0.0019$: also see the Supporting Information, Table S4 and Figure S6. Similar calculations for *trans*-$[Re_6S_8Cl_4(bpy)_2]^{2-}$ showed the substantially allowed lowest-energy absorption transitions as HOMO → LUMO+2 (35%)/HOMO−1 → LUMO+2 (30%)/HOMO−2 → LUMO+1 (16%) with $f = 0.0006$ and HOMO−1 → LUMO+2 (36%)/HOMO → LUMO+2 (26%)/HOMO−4 → LUMO+1 (16%) with $f = 0.0011$. Therefore, the substantially allowed lowest-energy absorption transitions in $[\mathbf{2a}]^{2-}$ or $[\mathbf{5a}]^{2-}$ possess a Re_6S_8 core-to-N-hetero-aromatic ligand MLCT character.

Table 5. Calculated Energies and Components of MOs near Frontier Orbital Levels for $[\mathbf{2a}]^{2-}$

	energy/eV	Re	S	Cl	ppy
LUMO+4	−1.85	0.83	0.14	0.03	0
LUMO+3	−1.89	0.82	0.16	0.01	0.01
LUMO+2	−2.05	0.19	0.07	0.02	0.72
LUMO+1	−2.25	0.41	0.09	0.01	0.48
LUMO	−2.39	0.99	0	0	0.01
HOMO	−5.96	0.72	0.28	0	0
HOMO−1	−5.99	0.73	0.27	0	0
HOMO−2	−6.35	0.28	0.45	0.27	0
HOMO−3	−6.41	0.32	0.34	0.34	0
HOMO−4	−6.41	0.07	0.63	0.29	0
HOMO−5	−6.44	0.32	0.34	0.33	0

Table 6. Calculated Energies and Components of MOs near Frontier Orbital Levels for $[\mathbf{5a}]^{2-}$

	energy/eV	Re	S	Cl	bpy
LUMO+4	−1.86	0.83	0.14	0.03	0
LUMO+3	−1.90	0.82	0.16	0.01	0.01
LUMO+2	−2.34	0.09	0.04	0.01	0.86
LUMO+1	−2.40	0.93	0	0	0.07
LUMO	−2.46	0.30	0.06	0	0.64
HOMO	−5.98	0.72	0.28	0	0
HOMO−1	−6.00	0.73	0.27	0	0
HOMO−2	−6.36	0.28	0.45	0.27	0
HOMO−3	−6.42	0.07	0.63	0.30	0
HOMO−4	−6.42	0.32	0.33	0.35	0
HOMO−5	−6.45	0.32	0.35	0.33	0

The results of the TD-DFT calculations are worth comparing with the absorption spectra of $[\mathbf{2a}]^{2-}$and $[\mathbf{5a}]^{2-}$. The absorption spectra of $[\mathbf{2a}]^{2-}$, $[\mathbf{3a}]^{2-}$, and $[\mathbf{5a}]^{2-}$ in acetonitrile are shown in the Supporting Information, Figure S8, and those of $[\mathbf{2b}]^{2-}$, $[\mathbf{3b}]^{2-}$, and $[\mathbf{5b}]^{2-}$ in acetonitrile are shown in the Supporting Information, Figure S9. While the lowest-energy absorption edges of the ppy and bpy complexes, $[\mathbf{2a,b}]^{2-}$ and $[\mathbf{5a,b}]^{2-}$, are extended to wavelength regions longer than 550 nm, those of the bpe complexes $[\mathbf{3a,b}]^{2-}$ were observed in wavelength regions shorter than 550 nm. It is noteworthy that the bpe ligand possesses no low-energy lying π^* orbital; this is different from the case of ppy or bpy. Thus, the absorption edge extending over 550 nm observed for $[\mathbf{2a,b}]^{2-}$ or $[\mathbf{5a,b}]^{2-}$ could be due to the MLCT character involving the low-energy lying π^* orbital of ppy or bpy, respectively. The simulated electronic absorption spectra of $[\mathbf{2a}]^{2-}$ and $[\mathbf{5a}]^{2-}$ (Supporting Information, Figures S10 and S11) agreed well with the observed spectra as seen in the Supporting Information, Figures S12 and S13, respectively. Therefore, we conclude that the absorption

(70) Deluzet, A.; Duclusaud, H.; Sautet, P.; Borshch, S. A. *Inorg. Chem.* **2002**, *41*, 2537–2542.

(71) We have carried out the calculation for $[Re_6S_8Cl_6]^{4-}$ by using the present method. The results are similar to those of the previously reported calculations. Namely, the occupied orbitals around the HOMO were mainly composed of the hexarhenium and the face capping sulfide. The unoccupied orbitals around the LUMO were composed mainly of the metal centers of the Re_6S_8 core.

edge extending above 550 nm observed for $[Re_6S_8Cl_4L_2]^{2-}$ (L = ppy or bpy) is assigned to the superposition of the Re_6S_8 core-to-N-heteroaromatic ligand CT and Re_6S_8 core-centered electronic transitions.[72] These conclusions also agree well with the spectroscopic and photophysical properties of the complexes as described below.

(3). Excited-State Properties of Hexarhenium(III) Complexes with Redox-active N-heteroaromatic Ligands. The photophysical properties described above clearly indicate that the excited states of the bis(bpy) complexes $[\mathbf{5a,b}]^{2-}$ are different from those of $[\mathbf{1}]^-$, $[\mathbf{2a,b}]^{2-}$, $[\mathbf{3a,b}]^{2-}$, $[\mathbf{4}]^-$, and other core-centered emissive hexarhenium complexes, $[Re_6S_8X_6]^{4-}$ and $[Re_6S_8Cl_{6-n}L_n]^{n-4}$ (n = 2, 3, L = py; n = 2, L = mpy). Therefore, we first discuss the excited-state properties of $[\mathbf{5a,b}]^{2-}$. Our electrochemical studies demonstrate that the bpy ligand reduction waves of the bis(bpy) complexes $[\mathbf{5a,b}]^{2-}$ are observed at around −1.45 V (vs Ag/AgCl), as mentioned before, which indicates that these complexes possess the bpy ligand-centered LUMO. It follows that the emissive excited states of $[\mathbf{5a,b}]^{2-}$ are best characterized by the bpy ligand-centered LUMO and the complexes should exhibit MLCT-like emissions. Similarly, the emissions from the bis(pz) complexes $[\mathbf{6a,b}]^{2-}$ reported previously will be also assigned to MLCT-like emissions, since these complexes show the emission characteristics and ligand-centered redox waves similar to those of $[\mathbf{5a,b}]^{2-}$. TD-DFT calculations for $[\mathbf{5a}]^{2-}$ indicate the predominantly bpy ligand-oriented LUMO and this further supports our assertion that the emission is MLCT type. In the case of MLCT emission from a transition metal complex represented by polypyridine ruthenium(II), the emission energy is sometimes discussed on the basis of the energy difference between the oxidation (E_{ox}, metal-centered: HOMO energy) and reduction potentials (E_{red}, ligand-centered: LUMO energy) of the complex: $\Delta E_{redox} = E_{ox} - E_{red}$.[73] In practice, a linear relationship between the MLCT emission energy and ΔE_{redox} has been observed for a series of polypyridine ruthenium(II) complexes with a slope value of about 1.0. In the case of the present MLCT emissions, E_{ox} and E_{red} are the Re_6S_8 core-oxidation and N-heteroaromatic ligand-reduction potentials, respectively. The ΔE_{redox} value of a hexarhenium(III) complex estimated by the present study was plotted against the emission energy of the relevant complex. As seen in Figure 5, we obtained a linear correlation between ΔE_{redox} and the emission energy for $[\mathbf{5a,b}]^{2-}$ and $[\mathbf{6a,b}]^{2-}$ with a slope value of 0.92. The results shown in Figure 5 straightforwardly proves the MLCT characters of the emissions from $[\mathbf{5a,b}]^{2-}$ and $[\mathbf{6a,b}]^{2-}$. The increasing emission lifetime of $[\mathbf{5a,b}]^{2-}$ in the solid state is reasonable, since the original strong emissions are not efficiently quenched in the solid state because of the lack of solvation.

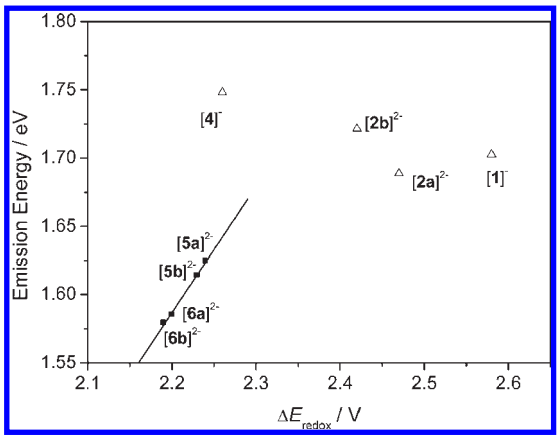

Figure 5. Plot of ΔE_{redox} for $[Re_6S_8Cl_4L_2]^{2-}$ (L = bpy, pz) (filled square) and $[Re_6S_8Cl_{6-n}(ppy)_n]^{n-4}$ (n = 2, 3) and $[Re_6S_8Cl_3(bpy)_3]^-$ (open triangle) against emission energy.

The complexes $[\mathbf{5a,b}]^{2-}$ showed relatively sharp emission spectra in the solid phase at 298 K with fwhm of 3100−3270 cm^{-1} and shorter wavelength shifts upon cooling to 80 K. As stated above, these results are different from the emission properties of a hexarhenium(III) complex possessing the Re_6S_8 core-centered excited-state. It is predicted that the contribution of the π^* character of the N-heteroaromatic ligand to the excited-state results in a decrease in the spin−orbit coupling interaction, and thus leading to smaller zero-field splitting energies between the emitting excited-state spin sublevels as compared with those in $[Re_6S_8X_6]^{4-}$. In the present stage of the investigation, we suppose that this will be the primary origin of the small fwhm and anomalous T-dependent emission of $[\mathbf{5a,b}]^{2-}$. By considering the participation of the Re_6S_8 core-to-bpy CT in the excited states of $[\mathbf{5a,b}]^{2-}$, one can also explain the large red shift of the emission spectrum in acetonitrile as compared with that in the solid state. Namely, the MLCT excited states of $[\mathbf{5a,b}]^{2-}$ are stabilized in energy by solvation in acetonitrile, leading to the red-shifted emission of the hexarhenium(III) complexes in acetonitrile. Our initial suggestions that the emissions of the group B complexes are MLCT, which was based on their weak emissions, are also supported by these discussions. The solvation would induce efficient non-radiative decay of the excited-state through interactions with polar solvent molecules, which is observed generally for CT excited-state molecules. Therefore, the T- and solvent-dependences of the spectroscopic and photophysical properties of $[\mathbf{5a,b}]^{2-}$ can also be explained by assuming the contribution of the Re_6S_8 core-to-N-heteroaromatic ligand CT to the emitting excited state.

The emission characteristics of the bpe complexes $[\mathbf{3a,b}]^{2-}$ were very similar to those of $[Re_6S_8X_6]^{4-}$ (X = Cl, Br, I, CN, NCS) and $[Re_6S_8Cl_{6-n}L_n]^{n-4}$ (n = 2, 3, L = py; n = 2, L = mpy).[27,47,50−53,55] Since a ligand-based reduction wave and a Re_6S_8 core-to-bpe CT absorption band have not been observed in the case of $[\mathbf{3a,b}]^{2-}$, the emissive excited-states of these complexes are characterized by the Re_6S_8 core-centered excited triplet state; this adequately explains the spectroscopic and photophysical properties of the complexes in both solution and solid phases, as seen in Table 4. The excited-state properties of the ppy

(72) The transition energy of the lowest-energy band is larger ca. +0.5−0.8 eV than the measured absorption band. In the case that TD-DFT calculations not consider the solvent in the ppy and bpy complexes, the transition energies of the MLCT band are shifted to the lower-energy positions.

(73) *Inorganic Electronic Structure and Spectroscopy, Volume II: Applications and Case Studies*; Solomon, E. I., Lever, A. B. P., Eds.; Wiley: New York, 1999.

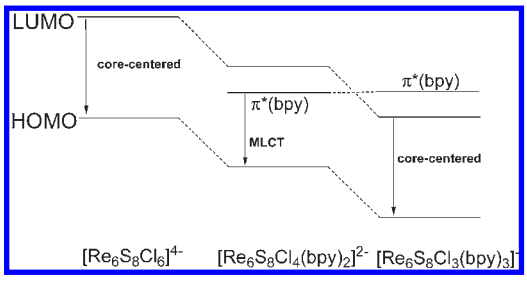

Figure 6. Schematic view of the correlation between the Re_6S_8 core-centered and MLCT transitions with changes in the terminal-ligand combinations.

complexes $[\mathbf{1}]^-$ and $[\mathbf{2a,b}]^{2-}$, and the tris(bpy) complex $[\mathbf{4}]^-$ might be considered as marginal cases between the Re_6S_8 core-centered and MLCT excited states. TD-DFT calculations for $[\mathbf{2a}]^{2-}$ revealed considerable mixing between the ligand π^* and metal orbitals in the Re_6S_8 core. The contributions of the metal orbitals to the excited state of $[\mathbf{2a}]^{2-}$ will be somewhat higher than those of $[\mathbf{5a}]^{2-}$. Although the ligand-centered reduction waves and the rather sharp emission bands in the solid states observed for $[\mathbf{2a,b}]^{2-}$ suggest that the excited states of the complexes show MLCT-like emission, other photophysical properties of $[\mathbf{2a,b}]^{2-}$ are similar to the Re_6S_8 core-centered excited states. Obviously, the energy level order of the Re_6S_8 core-centered and N-heteroaromatic ligand-centered states in the excited state would be somewhat modified from that in the ground state. Therefore, it can be concluded that the emissive excited states of $[\mathbf{2a,b}]^{2-}$ are the inseparable mixture of the MLCT and Re_6S_8 core-centered excited states. The tris(ppy) $[\mathbf{1}]^-$ and tris(bpy) $[\mathbf{4}]^-$ complexes may have less MLCT character. The Re_6S_8 core-centered oxidation waves of $[\mathbf{1}]^-$ and $[\mathbf{4}]^-$ appeared at more positive potentials than those of the bis-complexes as the number of N-heteroaromatic ligands increased. Namely, the Re_6S_8 core-centered HOMO levels are lowered as the number of N-heteroaromatic ligands in the complex increased. It is reasonable to assume that empty metal center orbitals are also lowered. If the N-heteroaromatic ligand π^* orbital remains constant in terms of energy, the LUMO possesses a greater metal character than that of the bis(N-heteroaromatic ligand) complex, as shown schematically in Figure 6. Therefore, the excited states of the tris(ppy) and tris(bpy) complexes possess considerably higher Re_6S_8 core-oriented character. The assertion that the MLCT character in the tris-complexes has less extent is supported by the fact that the data points of these complexes are away from the straight line of the ΔE_{redox} versus emission maximum energy plot shown in Figure 5.

Conclusions

The spectroscopic and photophysical properties of the hitherto reported hexarhenium(III) complexes have been discussed experimentally and theoretically in terms of the Re_6Q_8 (Q = S or Se) core-centered excited state. In the present study, we showed for the first time that *trans*/*cis*-$[Re_6S_8Cl_4L_2]^{2-}$ (L = bpy ($[\mathbf{5a,b}]^{2-}$) or pz ($[\mathbf{6a,b}]^{2-}$)) exhibited Re_6S_8 core-to-L charge transfer (MLCT) emissions, as demonstrated explicitly by the linear relationship between the emission maximum energies and the ΔE_{redox} ($= E_{ox} - E_{red}$) values for these four complexes (Figure 5). The HOMO ($\sim E_{ox}$)−LUMO ($\sim E_{red}$) energy gap of $[Re_6S_8Cl_4L_2]^{2-}$ corresponding to the emission maximum energy is determined primarily by the reduction potential of the bpy or pz ligand in the relevant Re_6S_8 complex. The anomalous solvent- and *T*-dependent emission characteristics of $[Re_6S_8Cl_4(bpy)_2]^{2-}$, which are totally different from those of the Re_6S_8 core-centered excited states of $[Re_6S_8X_6]^{4-}$ (X = Cl, Br, I) could also be explained by assuming the Re_6S_8 core-to-L CT excited states of $[Re_6S_8Cl_4L_2]^{2-}$. Therefore, the electron-accepting ability of an N-heteroaromatic ligand as L in $[Re_6S_8Cl_4L_2]^{2-}$ is of primary importance as the factor determining the spectroscopic and photophysical properties of the complexes. In practice, the Re_6S_8 complexes with bpe (1,2-bis(4-pyridyl)ethane) as a weak electron-accepting N-heteroaromatic ligand (i.e., $[\mathbf{3a,b}]^{2-}$) showed Re_6S_8 core-centered emissions similar to $[Re_6S_8X_6]^{4-}$. Therefore, all the present results of the spectroscopic and photophysical properties of $[Re_6S_8Cl_4L_2]^{2-}$ (L = bpy, ppy, or bpe) can be explained by the redox ability of an N-heteroaromatic ligand as L. We have also demonstrated that the emission is effectively quenched if the mechanism is MLCT type and if the ligand has free nitrogen sites ($[\mathbf{5a,b}]^{2-}$ and $[\mathbf{6a,b}]^{2-}$). In conclusion, we believe that an appropriate choice of an N-heteroaromatic terminal ligand controls the spectroscopic and photophysical characteristics of a hexarhenium(III) complex.

Supporting Information Available: Crystallographic data of $(Bu_4N)_2[\mathbf{2a}]$ and $(Bu_4N)_2[\mathbf{3a}]$ in CIF format, the discussion about the dependence of the redox potentials of the $Re(III)_6$/$Re(III)_5Re(IV)$ process on the type of terminal ligand and ligand−ligand redox interactions, a table of the atomic parameters used for the TD-DFT calculations of *trans*-$[Re_6S_8Cl_4(bpy)_2]^{2-}$, tables of the calculated energies and components of MOs near frontier orbital levels, tables of calculated excited-state energies, a figure of ^1H NMR spectra, figures of CVs of *mer*-$[Re_6S_8Cl_3(ppy)_3]^-$, *mer*-$[Re_6S_8Cl_3(bpy)_3]^-$, *trans*/*cis*-$[Re_6S_8Cl_4(L)_2]^{2-}$ (L = ppy, bpe), a figure of emission spectra for *trans*/*cis*-$[Re_6S_8Cl_4(bpe)_2]^{2-}$ in acetonitrile at 298 K, figures of selected MOs, figures of UV−vis absorption spectra in acetonitrile, figures of simulated and measured absorption spectra of *trans*-$[Re_6S_8Cl_4(ppy)_2]^{2-}$ and *trans*-$[Re_6S_8Cl_4(bpy)_2]^{2-}$ in acetonitrile, and a figure of a linear correlation between the pK_a of the free ligands and the redox potential of the complexes. This material is available free of charge via the Internet at http://pubs.acs.org.